Photochemical & Photobiological Sciences

PAPER

View Article Online
View Journal | View Issue

Cite this: *Photochem. Photobiol. Sci.*, 2014, **13**, 1590

Enhanced photocatalytic hydrogen production from an MCM-41-immobilized photosensitizer–[Fe–Fe] hydrogenase mimic dyad†

Wen Wang,[a] Tianjun Yu,*[a] Yi Zeng,[a] Jinping Chen,[a] Guoqiang Yang*[b] and Yi Li*[a]

Received 30th December 2013,
Accepted 2nd September 2014

DOI: 10.1039/c3pp50446h

www.rsc.org/pps

A covalently linked photosensitizer-catalytic center dyad Ps-Hy, consisting of two bis(2-phenylpyridine)(2,2′-bipyridine)iridium(III) chromophores (Ps) and a diiron hydrogenase mimic (Hy) was constructed by using click reaction. Ps-Hy was incorporated into K^+-exchanged molecular sieve MCM-41 to form a composite (Ps-Hy@MCM-41), which has been successfully applied to the photochemical production of hydrogen. The catalytic activity of Ps-Hy@MCM-41 is ~3-fold higher as compared with that of Ps-Hy in the absence of MCM-41. The incorporation of Ps-Hy into MCM-41 stabilizes the catalyst, and consequently, advances the photocatalysis. The present study provides a potential strategy for improving catalytic efficiency of artificial photosynthesis systems using mesoporous molecular sieves.

Introduction

The requirement to develop clean and sustainable sources of energy has stimulated new approaches to mimic natural photosynthesis in the conversion and storage of solar energy.[1–3] Of these approaches, the photochemical production of hydrogen from water is at the forefront. In nature, the interconversion of protons and hydrogen is efficiently catalyzed by metalloenzymes known as hydrogenases which exist in many microorganisms, and photoinduced electron transfer plays a central role.[4,5] The electron transfer processes develop a large separation of positive and negative charges within photosystem I (PSI) reaction centers.[6] The maintenance of this charge separation is critical for ensuing biochemical reactions.[7–10] By "mimicking" natural photosynthesis, chemists have tried to duplicate the hydrogen production events in photosynthesis with model compounds, which have been used as artificial photosynthetic systems for the conversion of solar energy.[11–17] Because of the fundamentality of photoinduced electron transfer to these systems, much effort has been expended to understand the processes of photoinduced electron transfer, with the ultimate goal of achieving the efficiency and economy of artificial photosynthesis systems.

Effective charge separation has been considered to be a key factor for both natural photosynthesis and artificial photochemical conversion.[18–21] The vectorial or unidirectional photoinduced electron transfer through a co-operative interaction between the various components in well-ordered nature photosynthetic systems provide an effective charge separation. Inspired by natural photosynthetic systems, chemists have attempted to use organized molecular assemblies, layered materials, silica gels, microporous and mesoporous materials to stabilize the charge separated states.[22] Much effort from our research group in recent years has been devoted to dendritic mimics of the natural light harvesting complex for photochemical conversion.[23–26] Recently, we developed a series of dendritic [Fe–Fe] hydrogenase mimics with exceptional activity for the photochemical production of hydrogen.[27] The dendritic frameworks provide a distinct microenvironment to regulate the electron-transfer process and to stabilize the charge separated state, consequently advancing the photocatalysis.

The interest in mimicking natural photosynthesis urges to develop a simpler way to stabilize the charge separated state of the artificial photosynthesis systems. The ordered mesoporous molecular sieves, such as MCM-41, MCM-48, SBA-15, *etc.*,

[a]*Key Laboratory of Photochemical Conversion and Optoelectronic Materials, Technical Institute of Physics and Chemistry, Chinese Academy of Sciences, Beijing 100190, P. R. China. E-mail: yili@mail.ipc.ac.cn, tianjun_yu@mail.ipc.ac.cn; Tel: +86 10 82543518*

[b]*Beijing National Laboratory for Molecular Sciences (BNLMS), Key Laboratory of Photochemistry, Institute of Chemistry, Chinese Academy of Sciences, Beijing 100190, P. R. China. E-mail: gqyang@iccas.ac.cn; Tel: +86 10 82617263*

† Electronic supplementary information (ESI) available: Synthesis and characterization of Ps-Hy and the model compounds, estimation of the free energy change (ΔG) for different electron transfer routes, ^{1}H NMR and HR-MS spectra of Ps-Hy, diffuse reflectance spectra of K-MCM-41, Ps-Hy, and Ps-Hy@MCM-41, TGA of K-MCM-41 and Ps-Hy@MCM-41, DLS datum of K-MCM-41, FTIR spectra of Ps-Hy and Ps-Hy@MCM-41 before and after 2 h irradiation, photochemical production of hydrogen with various ratios of CH_3CN–H_2O, different pH values and different TEA concentrations, emission spectra of Ps-Hy@MCM-41 in the presence and absence of TEA, emission and excitation spectra of Ps, cyclic voltammogram of compound **3** and Ps-Hy, transient absorption spectra of Ps and Ps-Hy in the presence of TEA, kinetic trace of Ps, Ps@MCM-41, Ps-Hy and Ps-Hy@MCM-41 in the presence of TEA, electrochemical data for PS, compound **3** and Ps-Hy, lifetimes for Fe^IFe^0 and $Ir(ppy)_2(bpy)$ in the presence and absence of K-MCM-41. See DOI: 10.1039/c3pp50446h

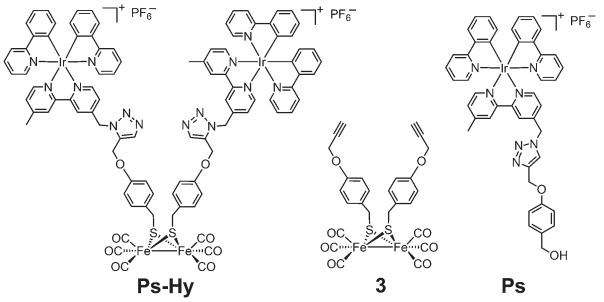

Fig. 1 Structures of dyad Ps-Hy, models **3** and Ps (asymmetry of the sulfur–carbon bond for the catalytic center is omitted).

display advantages such as tunable pore diameters (2–30 nm), narrow pore size distributions, high surface areas and electrostatic microenvironments, and have shown the ability of stabilizing the charge separated state.[28–35] Herein, we report a photosensitizer–[Fe–Fe]-hydrogenase mimic dyad (Ps-Hy, Fig. 1), which was incorporated into the ordered mesoporous K^+-exchanged molecular sieve MCM-41 to form a MCM-41-confined photosensitizer–[Fe–Fe]-hydrogenase mimic dyad (Ps-Hy@MCM-41). The studies on the photochemical production of hydrogen by Ps-Hy@MCM-41 and Ps-Hy demonstrate that the catalytic ability is improved by immobilization on MCM-41.

Experimental section

Materials

Reagents were purchased from Acros, Alfa Aesar, or Beijing Chemicals and were used without further purification unless otherwise noted. Mesoporous molecular sieve MCM-41 (SiO_2/Al_2O_3 mol/mol ≥ 20, BET ≥ 900 m^2 g^{-1}, d = 3.5 nm) was purchased from Xian Feng Nano Company. HPLC-grade acetonitrile was used for the photochemical production of hydrogen and photophysical studies. Milli-Q deionized water (Millipore) was used in the Ps-Hy@MCM-41 preparation, the light-driven hydrogen generation experiments and the spectroscopy measurements. Methanol and tetrahydrofuran were dried with sodium and distilled under a N_2 atmosphere.

Instrumentation

^{1}H NMR (400 MHz) spectra were recorded on a Bruker Avance Π-400 spectrometer with tetramethylsilane as an internal standard. Infrared spectra were recorded on a Nicolet NEXUS 670 FTIR spectrometer. ESI mass spectra were recorded on a Waters GCT Premier XE apparatus. Absorption and emission spectra were recorded on a Shimadzu UV-1601PC spectrometer and a Hitachi F-4500 spectrometer, respectively. UV-Vis reflectance spectra were recorded on a Shimadzu UV-VIS-3100 spectrophotometer. Thermogravimetric analysis (TGA) was performed on an SDT Q600 Simultaneous DSC-TGA instrument. The analysis of hydrogen production was carried out on a Shimadzu GC-2014 with a TCD detector. The electrochemical data were determined using glassy carbon electrodes on CHI600C. The transient absorption spectra were performed on an Edinburgh LP 920 pump–probe spectroscopic setup.

Preparation and characterization of Ps-Hy@MCM-41

K-MCM-41 was prepared by mixing silica–alumina molecular sieve MCM-41 (5 g) with potassium oxalate solution (0.25 M, 50 mL) and stirring for 6 h at room temperature (fresh potassium oxalate solution was replaced every 2 h). The resulting white solid was filtered, washed with water, dried and activated at 120 °C and 540 °C for 3 h, respectively. The following procedure was used to prepare Ps-Hy@MCM-41 by exchanging the potassium ion (K^+) with the cation of Ps-Hy. A small amount of K-MCM-41 (100.3 mg) was suspended in CH_3CN solution of Ps-Hy (1.0×10^{-4} M, 19 mL), which was stirred at ambient temperature overnight. The suspension was then centrifuged and the precipitate was dried at 40 °C under vacuum. The amount of Ps-Hy incorporated in K-MCM-41 was determined by the absorbance change at 340 nm ($\varepsilon = 3.0 \times 10^4$ M^{-1} cm^{-1}) of the supernatant before and after incorporation. Ps@MCM-41 was prepared and characterized similarly as Ps-Hy@MCM-41 except by using Ps instead of Ps-Hy.

Electrochemistry

A three-electrode system (a 3 mm glass carbon working electrode, a platinum wire counter electrode, and a non-aqueous Ag/Ag^+ reference electrode) was used to measure the cyclic voltammograms. The working electrode was polished with a 0.05 μm alumina paste and sonicated in acetone for 15 min before use. The electrolyte solution with 0.1 M n-Bu_4NPF_6 was purged with argon for 30 min before measurement. Electrochemical measurements were recorded at a scan rate of 100 mV s^{-1} and the ferrocene/ferrocenium redox couple (Fc/Fc^+) was used as a standard.

Photocatalytic H_2 generation

All experiments of photochemical production of hydrogen were performed in a Pyrex reactor with 10 mL sample solution and a magnetic stirrer. The sample solutions were purged with nitrogen for 30 min prior to irradiation. A 300 W Xe lamp was used as the visible light source with filters cutting off the light below 400 nm and above 800 nm and a set of neutral density filters was used to adjust the irradiation intensity. The amount of generated photoproduct of H_2 was identified and quantified with a gas chromatograph equipped with a 5 Å molecular sieve column, N_2 carrier gas, and a thermal conductivity detector (TCD) with methane as an internal standard. The response factor of 1.52 for H_2/CH_4 was determined by calibration with known amounts of H_2 and CH_4 under the experimental conditions.

Results and discussion

Preparation and characterization of Ps-Hy and Ps-Hy@MCM-41

An iridium complex $[Ir(ppy)_2(bpy)]PF_6$ (ppy = 2-phenylpyridine, bpy = 4,4′-dimethyl-2,2′-bipyridine) and a $\{(\mu\text{-}S_2)Fe_2(CO)_6\}$ subunit, one of the most common and primitive [2Fe2S] clusters used in mimics of the active site of diiron hydrogenase, were chosen as the photosensitizer and the catalyst center, respectively. The click reaction was used to connect the photosensitizer and the catalytic unit because of its mild reaction conditions and efficiency. The photosensitizer–diiron hydrogenase mimic dyad Ps-Hy was constructed using azido-substituted $[Ir(ppy)_2(bpy)]PF_6$ (compound **4**, ppy = 2-phenylpyridine, bpy = 4-(azidomethyl)-4′-methyl-2,2′-bipyridine) and alkynyl-substituted $\{(\mu\text{-}S_2)Fe_2(CO)_6\}$ (compound **3**) as the starting materials with reasonable yield (see Fig. S1 in the ESI†). As a model compound of photosensitizer (Ps), Ps was synthesized using 4-(2-propyn-1-yloxy)benzyl alcohol (compound **1**) instead of compound **3** with the same procedure described for Ps-Hy. The details of the synthesis and the characterization of **3**, **4**, Ps-Hy and Ps are described in the ESI.† The structures of the dyad Ps-Hy and the model compounds of a photosensitizer and a catalytic center (Ps and **3**) are depicted in Fig. 1, which were characterized by ^{1}H NMR and IR spectroscopy as well as mass spectrometry (see the ESI†).

The K^+-exchanged MCM-41 (K-MCM-41) was prepared according to a reported method using potassium oxalate as the K^+ source.[36] K-MCM-41 was further ion-exchanged with Ps-Hy to give the Ps-Hy@MCM-41 composite. The cation-exchange with $Ps\text{-}Hy^{2+}$ occurs spontaneously once K-MCM-41 mixed with Ps-Hy in CH_3CN, and the quantity of Ps-Hy incorporated with K-MCM-41 can be evaluated by the absorbance change of the supernatant (Fig. 2). The loading of Ps-Hy onto K-MCM-41 makes the color of K-MCM-41 change from white to yellow. The firmness of Ps-Hy loaded onto K-MCM-41 was examined by stirring the suspension of Ps-Hy@MCM-41 in CH_3CN at room temperature overnight. No leakage of Ps-Hy from Ps-Hy@MCM-41 was observed, which indicated that Ps-Hy was tightly incorporated into K-MCM-41. Similarly, Ps@MCM-41 was prepared using Ps instead of Ps-Hy.

Ps-Hy@MCM-41 was further characterized by DLS, UV-Vis, DRS-UV-Vis and FTIR spectroscopy as well as thermogravimetric analysis. The average diameter of the Ps-Hy@MCM-41 particles is 4.7 μm according to the DLS measurement (see Fig. S5 in the ESI†), which is in good agreement with the datum provided by the supplier (3–5 μm). Obvious light scattering was observed in the K-MCM-41 and Ps-Hy@MCM-41 suspensions because the molecular sieve is not on the nanoscale. The absorption spectrum of the Ps-Hy@MCM-41 suspension in CH_3CN is similar to the sum of those of Ps-Hy and K-MCM-41 with absorption bands at 254 and 340 nm characteristics of Ps-Hy (Fig. 3a). The diffuse reflectance spectrum of Ps-Hy@MCM-41 also exhibits the absorption bands of Ps-Hy (see Fig. S6 in the ESI†). Three prominent bands of the CO stretching vibration at 2070, 2033, and 1933 cm^{-1} attributed to Ps-Hy are observed in the FTIR spectrum of Ps-Hy@MCM-41 (Fig. 3b). The characterization results validate the reality of the incorporation of Ps-Hy into K-MCM-41. The thermogravimetric analysis further strengthens the fact of the formation of

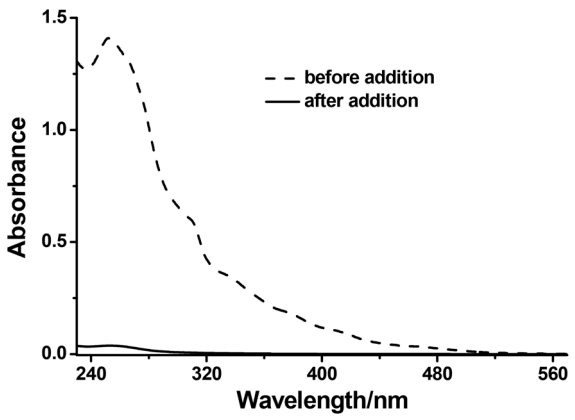

Fig. 2 Absorption spectra of Ps-Hy (10 μM) in CH_3CN solution and the supernatant (10 fold diluted) after addition of K-MCM-41 (K-MCM-41 (100.3 mg) was added to the Ps-Hy CH_3CN solution (1.0×10^{-4} M, 19 mL)).

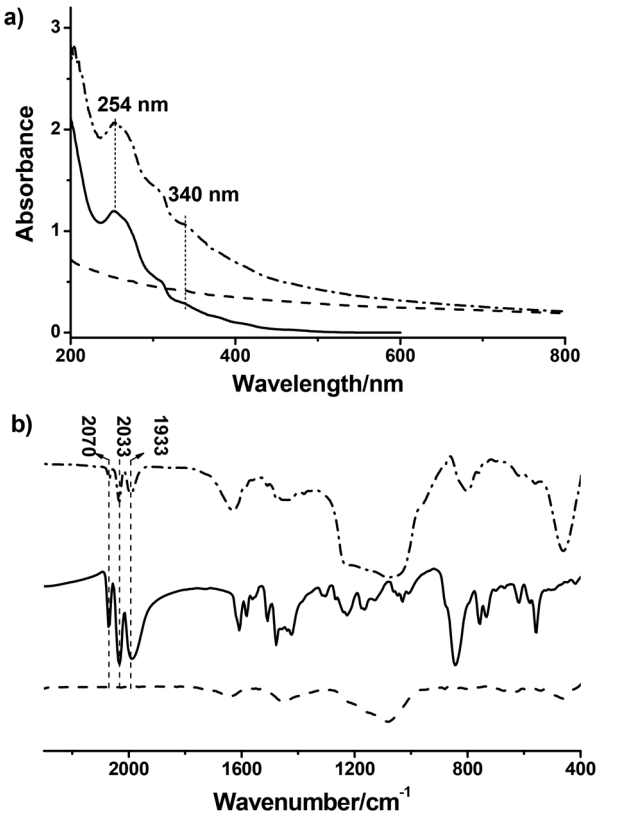

Fig. 3 (a) Absorption spectra of suspensions of K-MCM-41 (3.8 mg, dash line) and Ps-Hy@MCM-41 (3.8 mg, loading 77.8 μmol g^{-1}, dash dot line) in 5 mL CH_3CN, Ps-Hy (1×10^{-5} M, solid line) in CH_3CN. (b) FTIR spectra of K-MCM-41 (dash line), Ps-Hy@MCM-41 (dash dot line), and Ps-Hy (solid line).

Ps-Hy@MCM-41. Three distinct stages of weight loss (50–150 °C: 7.2%, 300–450 °C: 6.0% and 450–800 °C: 5.8%) were observed, which represent the desorption of water and the carbonyl ligands attached to the [2Fe2S] centers, the decomposition of the remaining part of Ps-Hy and the water loss *via* condensation of the silanol groups to form siloxane bonds, respectively (see Fig. S7 in the ESI†).[37–39]

Application of Ps-Hy@MCM-41 to hydrogen production

The catalytic performance of Ps-Hy@MCM-41 for light-driven hydrogen production was examined using triethylamine (TEA) as the sacrificial electron donor (Fig. 4). A solvent mixture of CH_3CN and H_2O was used to solubilize or disperse all the components. Irradiation of the catalyst system with visible light resulted in the production of hydrogen, which was identified and quantified by gas chromatography. Control experiments indicated that Ps-Hy and TEA are all essential for production of H_2, and the absence of any of them lead to no detectable photochemical production of H_2. The performance of the photocatalyst system was dramatically affected by the reaction conditions, such as the pH value, the water content of the solvent mixture, and the concentration of TEA.

To optimize the experimental conditions, light-induced hydrogen production was conducted using Ps-Hy@MCM-41 in CH_3CN–H_2O binary solvent with varied ratios of CH_3CN–H_2O, and at different pH values and different concentrations of TEA upon the visible light irradiation (Table 1). The optimal ratio of CH_3CN–H_2O was examined to be 9/1 (v/v) to achieve the best catalytic performance when all other conditions were kept identical (see Fig. S8 in the ESI†). The pH value of the catalytic system was adjusted by hydrochloric acid prior to irradiation. The best catalytic performance of the catalytic system was accomplished at the pH value of 10 with the same amount of Ps-Hy@MCM-41 (5.5 mg Ps-Hy@MCM-41 with loading 19.1 μmol g^{-1}) and the same concentration of TEA ([TEA] = 0.6 M) in CH_3CN–H_2O (9/1, v/v) (see Fig. S9 in the ESI†). The poorer catalytic performance of the catalytic system at lower and higher pH values may be rationalized by the depressed ability of electron donation of TEA and the lower concentration of H^+, respectively. Keeping the optimal conditions of pH = 10 and CH_3CN–H_2O = 9/1 (v/v), an obvious improvement in photochemical production of hydrogen was observed when the concentration of TEA was successively increased from 0.4 M to 0.8 M (see Fig. S10 in the ESI†).

Table 1 Influence of the pH value, solvents, concentration of TEA on photoinduced H_2 evolution[a]

Run	pH	TEA (M)	Irrad. time (h)	H_2 production (μL)
1[b]	9	0.6	8	8.4 ± 0.5
2[b]	10	0.6	8	10.1 ± 0.6
3[b]	11	0.6	4	4.8 ± 0.2
4[c]	10	0.6	8	7.0 ± 0.3
5[d]	10	0.6	8	8.2 ± 0.4
6[b]	10	0.4	8	9.4 ± 0.4
7[b]	10	0.8	8	11.8 ± 0.7

[a] Runs 1–7 with Ps-Hy@MCM-41 (5.5 mg, Ps-Hy: 19.1 μmol g^{-1}, [Ps-Hy] = 10 μM) as a catalyst. [b] CH_3CN–H_2O = 9/1 (v/v). [c] CH_3CN–H_2O = 8/2 (v/v). [d] CH_3CN–H_2O = 9.5/0.5 (v/v).

To evaluate the effect of K-MCM-41 on the catalytic performance of Ps-Hy, the photochemical production of hydrogen of Ps-Hy@MCM-41 was conducted under the optimal reaction conditions with the TEA concentration of 0.8 M. The photocatalytic behavior of Ps-Hy in a homogeneous catalytic system was also examined under the same reaction conditions using the same amount of Ps-Hy. Upon 8 h irradiation, 11.8 μL H_2 was generated from the Ps-Hy@MCM-41 catalytic system and only 4.4 μL H_2 was produced from the Ps-Hy homogeneous catalyst system (Fig. 5). The catalytic performance of Ps-Hy is evidently enhanced by immobilization into K-MCM-41.

The quantum yield of hydrogen production in the Ps-Hy@MCM-41 catalytic system was measured by irradiation of the suspension under the optimal reaction conditions (5.5 mg Ps-Hy@MCM-41, loading: 19.1 μmol g^{-1}, pH = 10, CH_3CN–H_2O = 9/1 (v/v)). A LED lamp (1 W, 440 nm) was used as the light source. At the period of the maximum rate of

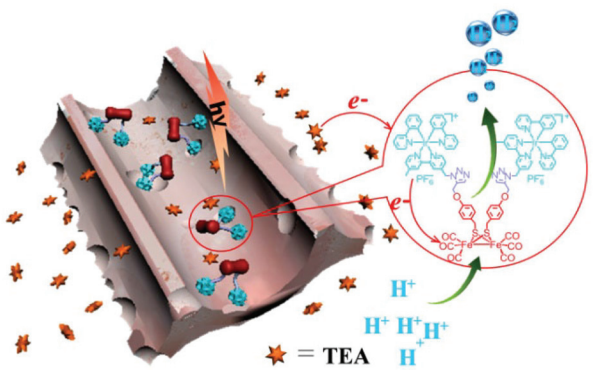

Fig. 4 Schematic illustration of the photochemical production of H_2 by Ps-Hy@MCM-41.

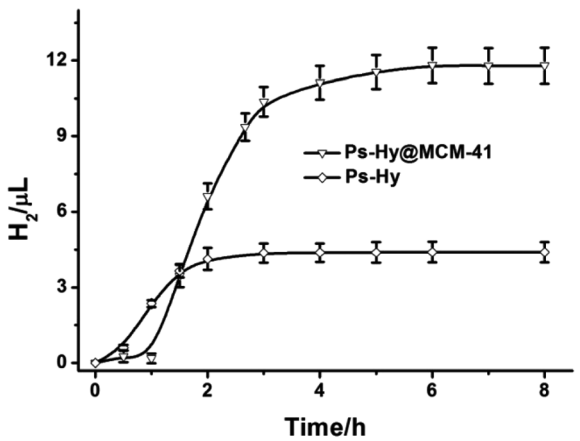

Fig. 5 Photochemical production of hydrogen by 5.5 mg Ps-Hy@MCM-41 (loading: 19.1 μmol g^{-1}) and Ps-Hy (10 μM) at the pH value of 10 in 10 mL CH_3CN–H_2O (9/1, v/v) upon irradiation with visible light.

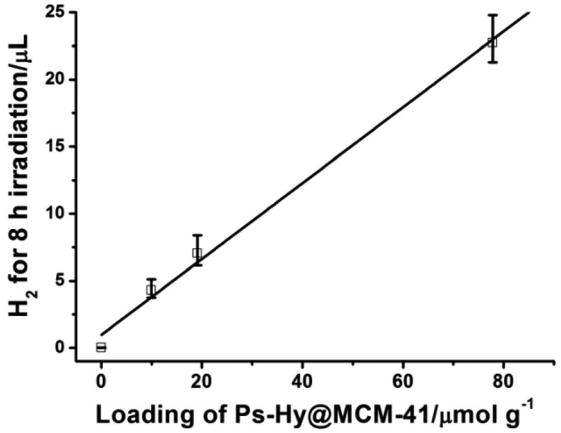

Fig. 6 Photocatalytic evolution of H_2 for 8 h irradiation by Ps-Hy@MCM-41 with different loading in 10 mL CH_3CN–H_2O (9/1, v/v) at the pH value of 11.9. Ps-Hy@MCM-41 = 5.5 mg, [TEA] = 0.6 M.

hydrogen evolution, the quantum yield was determined to be 3%, which means that of 100 photons absorbed by the photosensitizer, 3 photons are stored as the chemical energy. This number is analogous with that reported in most of the literature reports, and only a few hydrogen production systems based on [2Fe2S]-catalysts can achieve higher quantum yields so far.[27,40,41]

To clarify the reason of enhanced catalytic performance in the Ps-Hy@MCM-41 catalytic system, the FTIR spectra of the catalytic systems before and after 2 h irradiation were recorded (see Fig. S11 in the ESI†). After two hours irradiation, three prominent bands at 2070, 2033, and 1933 cm^{-1} assigned to the CO stretching vibration disappeared completely in the homogenous Ps-Hy catalytic system and remained in the Ps-Hy@MCM-41 catalytic system. This indicates that Hy decomposed during the irradiation and the immobilization of Ps-Hy into K-MCM-41 can lower the photo-destruction rate of the hydrogenase mimic, which prolongs the life of Hy in the Ps-Hy@MCM-41 catalytic system.

Generally, the catalysts such as the [Fe–Fe] hydrogenase mimics show better catalytic performance at lower concentrations because the catalysts can absorb light and decompose gradually during the illumination.[27] The photochemical production of hydrogen by Ps-Hy@MCM-41 with different loading was proceeded in CH_3CN–H_2O (9/1, v/v), and the results for 8 h irradiation are shown in Fig. 6. Interestingly, the overall evolution of H_2 increases linearly with the loading (10–80 μmol g^{-1}) when all the other conditions are kept identical. This character benefits the catalytic performance of catalysts at higher concentrations, giving the potentials for the magnified production.

Mechanisms of the photochemical production of hydrogen and the enhanced catalytic activity of Ps-Hy@MCM-41

The photocatalytic H_2 evolution of homogeneous three-component systems involves a photosensitizing mechanism which begins with the excitation of a photosensitizer followed by an electron delivery to the catalyst either through a direct oxidative quenching or after reduction by the sacrificial electron donor.[42] The thermodynamic feasibility of two different cases was analyzed by estimating the free energy change ΔG to clarify the electron transfer mechanism of catalysis. The ΔG of direct electron transfer from the excited photosensitizer Ps to the [2Fe2S] catalytic center Hy involved in an electron transfer process was estimated to be positive (0.02 eV), which indicated that such an endothermic pathway would be inefficient if any did occur. Alternatively, Ps can be reductively quenched by TEA generating a reduced photosensitizer Ps^- even in the form of Ps-Hy@MCM-41 (see Fig. S12 in the ESI†), which is sufficiently reductive to donate an electron to the [2Fe2S] center (*i.e.* Fe^IFe^I) generating $[2Fe2S]^-$ (*i.e.* Fe^0Fe^I) based on the ΔG (−0.27 eV) given by the reduction potentials. Further reduction of the reduced core $[2Fe2S]^-$ to $[2Fe2S]^{2-}$ (*i.e.* Fe^0Fe^0) is thermodynamically unfeasible owing to its very negative reduction potential (Table S1†). Therefore, we infer that the electron transfer occurs between the reduced photosensitizer and the [2Fe2S] catalytic center, which is further validated by the transient absorption spectroscopy studies.

Pulsed laser photolysis of Ps-Hy and Ps-Hy@MCM-41, and their model compounds Ps and Ps@MCM-41 in the presence of TEA was performed in deaerated CH_3CN–H_2O (9/1, v/v, 5 mL) using a 420 nm excitation light. The transient absorption spectra of the Ps@MCM-41 and Ps-Hy@MCM-41 systems are quite similar. The intensive transient absorption bands at around 390, 500 and 530 nm were readily formed as shown in Fig. 7 and S15,† which are assigned to the reduced species Ps^- by reference to the transient absorption of the reduced species of Ir(III) complex.[27] The transient absorption band of $[2Fe2S]^-$ around 400 nm[43] could not be observed clearly, which might be caused by the low transient absorption coefficient of $[2Fe2S]^-$ and the overlap of the transient absorption of Ps^- and $[2Fe2S]^-$. Control experiments in the absence of TEA show

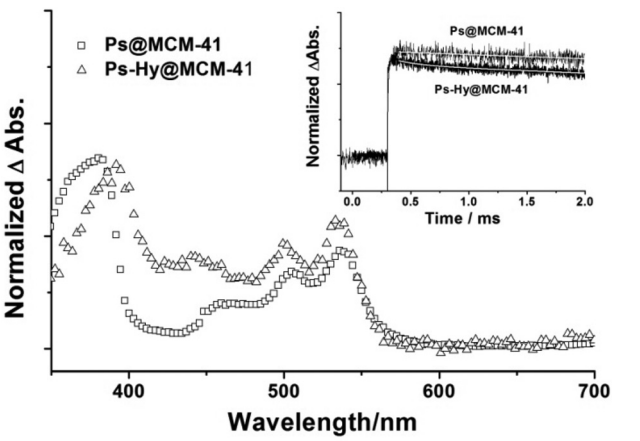

Fig. 7 Transient absorption spectra of Ps@MCM-41 (3.0 mg, loading: 60 μmol g^{-1}) and Ps-Hy@MCM-41 (3.0 mg, loading: 77.8 μmol g^{-1}) with TEA (0.8 M) at the pH value of 10 in 5 mL deaerated CH_3CN–H_2O = 9/1 (v/v) at 50 μs after the laser pulse. Inset: kinetic traces of Ps@MCM-41 and Ps-Hy@MCM-41 at 530 nm.

no formation of Ps^- in either Ps-Hy or the Ps-Hy@MCM-41 catalytic system, confirming that the excited photosensitizer is reductively quenched by the sacrificial electron donor. A subsequent oxidization of Ps^- was further validated by the shortened lifetimes of the reduced photosensitizer in the presence of Hy (see below). After quenching the photosensitizer, TEA undergoes decomposition to produce a proton, acetaldehyde, and diethylamine in the presence of water.[44]

To understand the enhanced catalytic activity of Ps-Hy by MCM-41, the kinetics of the intermediate states was further studied by analyzing the transient absorption spectra. The lifetimes of the reduced photosensitizer (Ps^- and Ps^-@MCM-41) in the absence and presence of MCM-41 are 14.5 and 19.0 ms by fitting the decay trace at 530 nm mono-exponentially. In the Ps-Hy and Ps-Hy@MCM-41 dyad systems, the decay curves at 530 nm for the Ps-Hy and Ps-Hy@MCM-41 systems can only be fitted double-exponentially (see Table S2 in the ESI†). A fast decay (~6%) appears at the beginning of the decay curves and the repurification of Ps-Hy results in no change of the kinetics. Further studies on the transient absorption kinetics at 530 nm after 30 and 60 minutes irradiation demonstrate that the proportion of the fast decay increases with the irradiation time (Fig. S17, Table S2†). Thereby, the fast decay can be assigned to the unknown decomposition products of Ps-Hy caused by the transient photolysis. The obtained lifetime in milliseconds is assigned to Ps^- (3.0 and 4.4 ms for the Ps-Hy and Ps-Hy@MCM-41 systems, respectively) The shortened lifetime of Ps^- in the Ps-Hy and Ps-Hy@MCM-41 dyad systems substantiates the occurrence of the electron transfer from Ps^- to Hy. The rate constants of intramolecular electron transfer between Ps^- and Hy in the Ps-Hy and Ps-Hy@MCM-41 systems are calculated to be 262 and 175 s^{-1}, respectively, which are different from the result reported by Hammarström *et al.*[45] their reported catalytic system, the rate constant of the reaction of the reduced photosensitizer $[Ru(bpy)_3]^+$ with a similar [2Fe2S] catalyst in DMF–water is about two magnitude higher than those in ours work. Although the electron transfer process in the Ps-Hy@MCM-41 system is slower than that in the Ps-Hy system, the Ps-Hy@MCM-41 system shows better catalytic performance, which indicates that the electron transfer process from Ps- to Hy is not the rate-determining step in this hydrogen production system. The electron transfer processes from Ps^- to Hy in the absence and presence of MCM-41 show similar quenching efficiencies of Ps^- with the numbers 0.79 and 0.77 for the Ps-Hy and Ps-Hy@MCM-41 catalytic systems, respectively. The final production quantum yield of a few percent should be ascribed to the energy losses during the reductive quenching of *Ps by TEA, the oxidation of Ps^- by Hy, and the subsequent catalytic processes after reducing [2Fe2S] by Ps^-. Therefore, we speculate that the better performance of the Ps-Hy@MCM-41 catalytic system can be attributed to the stabilization effect of the molecular sieve, which is further verified by the kinetic studies of the transient absorption of the catalytic systems. The variation of the kinetics with irradiation time indicates that Hy-Ps decomposes gradually during the irradiation both in the absence and presence of MCM-41. The proportion of the fast decay assigned to the decomposition products of Ps-Hy increases with the irradiation time (Table S2†). The slower decomposition of Ps-Hy in the Ps-Hy@MCM-41 system indicates that the decomposition of Ps-Hy is evidently slowed down by immobilization into MCM-41, which is consistent with the results of FTIR studies.

Conclusions

A photosensitizer–[Fe–Fe] hydrogenase mimic dyad Ps-Hy was synthesized and immobilized into the mesoporous molecular sieve K-MCM-41 to form a composite Ps-Hy@MCM-41. The results of photochemical production of hydrogen with Ps-Hy and Ps-Hy@MCM-41 in CH_3CN–H_2O (9/1, v/v) using TEA as the sacrificial electron donor demonstrate that the catalytic activity is enhanced about three times by the immobilization of Ps-Hy into K-MCM-41. The immobilization of Ps-Hy into K-MCM-41 stabilizes the catalyst to a certain extent, and thus advances the photocatalysis. The present study provides a potential strategy for improving the catalytic efficiency of artificial photosynthesis systems using mesoporous molecular sieves.

Acknowledgements

Financial support from 973 Program (no. 2013CB834505, 2013CB834703) and the National Natural Science Foundation of China (no. 21302196, 21173245, 21233011 and 21273258) and the Solar Energy Initiative of the Chinese Academy of Sciences is gratefully acknowledged.

Notes and references

1 V. H. Grassian, G. Meyer, H. Abruña, G. W. Coates, L. E. Achenie, T. Allison, B. Brunschwig, J. Ferry, M. Garcia Garibay, J. Gardea Torresdey, C. P. Grey, J. Hutchison, C. J. Li, C. Liotta, A. Raguskas, S. Minteer, K. Mueller, J. Roberts, O. Sadik, R. Schmehl, W. Schneider, A. Selloni, P. Stair, J. Stewart, D. Thorn, J. Tyson, B. Voelker, J. M. White and F. Wood Black, Viewpoint: Chemistry for a sustainable future, *Environ. Sci. Technol.*, 2007, **41**, 4840–4846.
2 D. Gust, T. A. Moore and A. L. Moore, Solar fuels via artificial photosynthesis, *Acc. Chem. Res.*, 2009, **42**, 1890–1898.
3 J. Barber, Photosynthetic energy conversion: natural and artificial, *Chem. Soc. Rev.*, 2009, **38**, 185–196.
4 C. D. Tard and C. J. Pickett, Structural and functional analogues of the active sites of the [Fe]-, [NiFe]-, and [FeFe]-hydrogenases, *Chem. Rev.*, 2009, **109**, 2245–2274.
5 J. W. Peters, W. N. Lanzilotta, B. J. Lemon and L. C. Seefeldt, X-ray crystal structure of the Fe-only hydrogenase (cpl) from clostridium pasteurianum to 1.8 angstrom resolution, *Science*, 1998, **282**, 1853–1858.

6 E. S. Andreiadis, M. Chavarot-Kerlidou, M. Fontecave and V. Artero, Artificial photosynthesis: from molecular catalysts for light-driven water splitting to photoelectrochemical cells, *Photochem. Photobiol.*, 2011, **87**, 946–964.
7 G. Mcdermott, S. M. Prince, A. A. Freer, A. M. Hawthornthwaitelawless, M. Z. Papiz, R. J. Cogdell and N. W. Isaacs, Crystal-structure of an integral membrane light-harvesting complex from photosynthetic bacteria, *Nature*, 1995, **374**, 517–521.
8 T. Pullerits and V. Sundstrom, Photosynthetic light-harvesting pigment-protein complexes: toward understanding how and why, *Acc. Chem. Res.*, 1996, **29**, 381–389.
9 J. Deisenhofer, O. Epp, K. Miki, R. Huber and H. Michel, Structure of the protein subunits in the photosynthetic reaction center of rhodopseudomonas-viridis at 3 Å resolution, *Nature*, 1985, **318**, 618–624.
10 G. Feher, J. P. Allen, M. Y. Okamura and D. C. Rees, Structure and function of bacterial photosynthetic reaction centers, *Nature*, 1989, **339**, 111–116.
11 H. H. Cui, M. Q. Hu, H. M. Wen, G. L. Chai, C. B. Ma, H. Chen and C. N. Chen, Efficient FeFe hydrogenase mimic dyads covalently linking to iridium photosensitizer for photocatalytic hydrogen evolution, *Dalton Trans.*, 2012, **41**, 13899–13907.
12 S. Ott, M. Kritikos, B. Akermark and L. C. Sun, Synthesis and structure of a biomimetic model of the iron hydrogenase active site covalently linked to a ruthenium photosensitizer, *Angew. Chem., Int. Ed.*, 2003, **42**, 3285–3288.
13 A. P. S. Samuel, D. T. Co, C. L. Stern and M. R. Wasielewski, Ultrafast photodriven intramolecular electron transfer from a zinc porphyrin to a readily reduced diiron hydrogenase model complex, *J. Am. Chem. Soc.*, 2010, **132**, 8813–8815.
14 Y. Sano, A. Onoda and T. Hayashi, Photocatalytic hydrogen evolution by a diiron hydrogenase model based on a peptide fragment of cytochrome c(556) with an attached diiron carbonyl cluster and an attached ruthenium photosensitizer, *J. Inorg. Biochem.*, 2012, **108**, 159–162.
15 L. C. Song, M. Y. Tang, F. H. Su and Q. M. Hu, A biomimetic model for the active site of iron-only hydrogenases covalently bonded to a porphyrin photosensitizer, *Angew. Chem., Int. Ed.*, 2006, **45**, 1130–1133.
16 H. G. Cui, W. Mei, L. L. Duan and L. C. Sun, Preparation, characterization and electrochemistry of an iron-only hydrogenase active site model covalently linked to a ruthenium tris(bipyridine) photosensitizer, *J. Coord. Chem.*, 2008, **61**, 1856–1861.
17 S. Ott, M. Borgstrom, M. Kritikos, R. Lomoth, J. Bergquist, B. Akermark, L. Hammarstrom and L. C. Sun, Model of the iron hydrogenase active site covalently linked to a ruthenium photosensitizer: synthesis and photophysical properties, *Inorg. Chem.*, 2004, **43**, 4683–4692.
18 S. K. Choi, S. Kim, J. Ryu, S. K. Lim and H. Park, Titania nanofibers as a photo-antenna for dye-sensitized solar hydrogen, *Photochem. Photobiol. Sci.*, 2012, **11**, 1437–1444.
19 A. Magnuson, M. Anderlund, O. Johansson, P. Lindblad, R. Lomoth, T. Polivka, S. Ott, K. Stensjo, S. Styring, V. Sundstrom and L. Hammarstrom, Biomimetic and microbial approaches to solar fuel generation, *Acc. Chem. Res.*, 2009, **42**, 1899–1909.
20 P. Poddutoori, D. T. Co, A. P. S. Samuel, C. H. Kim, M. T. Vagnini and M. R. Wasielewski, Photoinitiated multistep charge separation in ferrocene-zinc porphyrin-diiron hydrogenase model complex triads, *Energy Environ. Sci.*, 2011, **4**, 2441–2450.
21 F. Y. Wen and C. Li, Hybrid artificial photosynthetic systems comprising semiconductors as light harvesters and biomimetic complexes as molecular cocatalysts, *Acc. Chem. Res.*, 2013, **46**, 2355–2364.
22 R. T. Koodali, Photoinduced charge separation in microporous and mesoporous materials, *Can. J. Chem.*, 2011, **89**, 257–265.
23 J. P. Chen, S. Y. Li, L. Zhang, B. N. Liu, Y. B. Han, G. Q. Yang and Y. Li, Light-harvesting and photoisomerization in benzophenone and norbornadiene-labeled poly(aryl ether) dendrimers via intramolecular triplet energy transfer, *J. Am. Chem. Soc.*, 2005, **127**, 2165–2171.
24 T. J. Yu, W. Wang, J. P. Chen, Y. Zeng, Y. Y. Li, G. Q. Yang and Y. Li, Dendrimer-encapsulated pt nanoparticles: an artificial enzyme for hydrogen production, *J. Phys. Chem. C*, 2012, **116**, 10516–10521.
25 Y. Zeng, Y. Li, M. Li, G. Q. Yang and Y. Li, Enhancement of energy utilization in light-harvesting dendrimers by the pseudorotaxane formation at periphery, *J. Am. Chem. Soc.*, 2009, **131**, 9100–9106.
26 Y. Zeng, Y. Y. Li, J. P. Chen, G. Q. Yang and Y. Li, Dendrimers: a mimic natural light-harvesting system, *Chem. – Asian J.*, 2010, **5**, 992–1005.
27 T. J. Yu, Y. Zeng, J. P. Chen, Y. Y. Li, G. Q. Yang and Y. Li, Exceptional dendrimer-based mimics of diiron hydrogenase for the photochemical production of hydrogen, *Angew. Chem., Int. Ed.*, 2013, **52**, 5631–5635.
28 M. Cai, R. Xiao, T. Yan and H. Zhao, A simple and green synthesis of diaryl sulfides catalyzed by an MCM-41-immobilized copper(I) complex in neat water, *J. Organomet. Chem.*, 2014, **749**, 55–60.
29 X. Feng, G. E. Fryxell, L. Q. Wang, A. Y. Kim, J. Liu and K. M. Kemner, Functionalized monolayers on ordered mesoporous supports, *Science*, 1997, **276**, 923–926.
30 S. Fukuzumi, K. Doi, A. Itoh, T. Suenobu, K. Ohkubo, Y. Yamada and K. D. Karlin, Formation of a long-lived electron-transfer state in mesoporous silica-alumina composites enhances photocatalytic oxygenation reactivity, *Proc. Natl. Acad. Sci. U. S. A.*, 2012, **109**, 15572–15577.
31 S. Fukuzumi and Y. Yamada, Shape- and size-controlled nanomaterials for artificial photosynthesis, *ChemSusChem*, 2013, **6**, 1834–1847.
32 C. T. Kresge, M. E. Leonowicz, W. J. Roth, J. C. Vartuli and J. S. Beck, Ordered mesoporous molecular-sieves synthesized by a liquid-crystal template mechanism, *Nature*, 1992, **359**, 710–712.
33 K. Mori, T. Yamaguchi, S. Ikurumi and H. Yamashita, Positive effects of the residual templates within the

MCM-41 mesoporous silica channels in the metal-catalyzed reactions, *Chem. Commun.*, 2013, **49**, 10468–10470.

34 Y. Yamada, A. Nomura, K. Ohkubo, T. Suenobu and S. Fukuzumi, The long-lived electron transfer state of the 2-phenyl-4-(1-naphthyl)quinolinium ion incorporated into nanosized mesoporous silica-alumina acting as a robust photocatalyst in water, *Chem. Commun.*, 2013, **49**, 5132–5134.

35 D. Y. Zhao, J. L. Feng, Q. S. Huo, N. Melosh, G. H. Fredrickson, B. F. Chmelka and G. D. Stucky, Triblock copolymer syntheses of mesoporous silica with periodic 50 to 300 angstrom pores, *Science*, 1998, **279**, 548–552.

36 X. Li, A. J. Wang, Y. Wang, Y. Y. Chen, Y. H. Liu and Y. K. Hu, Hydrodesulfurization of dibenzothiophene over Ni-Mo sulfides supported by proton-exchanged siliceous MCM-41, *Catal. Lett.*, 2002, **84**, 107–113.

37 S. Pullen, H. Fei, A. Orthaber, S. M. Cohen and S. Ott, Enhanced photochemical hydrogen production by a molecular diiron catalyst incorporated into a metal-organic framework, *J. Am. Chem. Soc.*, 2013, **135**, 16997–17003.

38 C. Y. Chen, H. X. Li and M. E. Davis, Studies on mesoporous materials .I. Synthesis and characterization of MCM-41, *Microporous Mater.*, 1993, **2**, 17–26.

39 C. A. Koh, R. Nooney and S. Tahir, Characterisation and catalytic properties of MCM-41 and pd/MCM-41 materials, *Catal. Lett.*, 1997, **47**, 199–203.

40 F. Wang, W. J. Liang, J. X. Jian, C. B. Li, B. Chen, C. H. Tung and L. Z. Wu, Exceptional poly(acrylic acid)-based artificial [FeFe]-hydrogenases for photocatalytic H_2 production in water, *Angew. Chem., Int. Ed.*, 2013, **52**, 8134–8138.

41 M. B. Wilker, K. E. Shinopoulos, K. A. Brown, D. W. Mulder, P. W. King and G. Dukovic, Electron transfer kinetics in CdS nanorod-FeFe-hydrogenase complexes and implications for photochemical H_2 generation, *J. Am. Chem. Soc.*, 2014, **136**, 4316–4324.

42 R. Lomoth and S. Ott, Introducing a dark reaction to photochemistry: photocatalytic hydrogen from [FeFe] hydrogenase active site model complexes, *Dalton Trans.*, 2009, 9952–9959.

43 Y. Na, J. X. Pan, M. Wang and L. C. Sun, Intermolecular electron transfer from photogenerated $Ru(bpy)_3^{+}$ to [2Fe2S] model complexes of the iron-only hydrogenase active site, *Inorg. Chem.*, 2007, **46**, 3813–3815.

44 A. J. Esswein and D. G. Nocera, Hydrogen production by molecular photocatalysis, *Chem. Rev.*, 2007, **107**(10), 4022–4047.

45 D. Streich, Y. Astuti, M. Orlandi, L. Schwartz, R. Lomoth, L. Hammarström and S. Ott, High-turnover photochemical hydrogen production catalyzed by a model complex of the [FeFe]-hydrogenase active site, *Chem. – Eur. J*, 2010, **16**, 60–63.